ELSEVIER

Journal of Nuclear Materials 245 (1997) 10–16

journal of nuclear materials

Crystal structure of thin oxide films grown on Zr–Nb alloys studied by RHEED

D. Khatamian *, S.D. Lalonde [1]

Reactor Materials Research Branch, Chalk River Laboratories, Chalk River, Ontario, Canada, K0J 1J0

Received 12 June 1996; accepted 18 December 1996

Abstract

The highly surface sensitive reflection high energy electron diffraction (RHEED) technique was used to determine the crystal structure of oxide films grown on Zr–Nb alloys in air up to 673 K. The results show that the oxide films grown on Zr–2.5 wt% Nb (α-Zr + β-Zr) have a mixture of nearly-cubic-tetragonal and monoclinic structures for films of 200 nm thick or less and that the outer layers of films thicker than 800 nm only have the monoclinic crystal structure. However, oxide films grown on Zr–20 wt% Nb (β-Zr) have a stabilized nearly-cubic-tetragonal structure for all film thicknesses, studied here, up to 2100 nm.

1. Introduction

Core components of nuclear power reactors are made of zirconium based alloys. To increase the lifetime of such components as much as possible, the rate of corrosion and hydrogen ingress into the components must be reduced. Both the corrosion rate and hydrogen ingress depend on the morphology, crystal structure, porosity and the chemical state of the oxide scales grown on the components. The oxide scales are known to be predominantly monoclinic (m) ZrO_2. Earlier studies [1,2] have shown that the oxide layer is under high compressive stress and it has been speculated that such stresses may stabilize the oxide in its tetragonal (t) form which is normally stable only at temperatures above 1400 K. More recent studies by Raman spectroscopy (RS) and X-ray diffraction (XRD) [3,4] have shown that the oxide is a mixture of both t and m ZrO_2 structures. Godlewski et al. [3], using tapered samples, have shown that in Zircaloy-4 and Zr–1 Nb (Zr–1 wt% Nb) alloys, ~ 40% of the oxide film near the oxide/metal interface has t structure and the proportion of t decreases to ~ 15% as the distance from the interface increases beyond ~ 600 nm.

In modern CANDU™ nuclear reactors, pressure tubes of cold-worked Zr–2.5 Nb (Zr–2.5 wt% Nb) material are used in the reactor core to contain the fuel bundles and the heavy water (D_2O) coolant [5]. The microstructure of the tubes comprises elongated α-Zr grains surrounded by a network of β-Zr containing Zr–20 Nb (Zr–20 wt% Nb). The β-Zr phase is unstable below ~ 890 K [6] and decomposes to α-Zr and β-Nb via $\beta\text{-Zr} \rightarrow \omega + \beta_{\text{Nb-enriched}} \rightarrow \alpha + \omega + \beta_{\text{Nb-enriched}} \rightarrow \alpha + \beta_{\text{Nb-enriched}} \rightarrow \alpha + \beta\text{-Nb}$ [7]. In the present investigation, we have used the reflection high energy electron diffraction (RHEED) technique to study the crystal structure of oxide films grown on Zr–2.5 Nb and Zr–20 Nb (β-Zr) alloys. RHEED is a highly surface sensitive technique and is able to sample materials within a depth of ~ 20 nm from the surface. The oxide films can also be examined in their as-formed state without further preparation, hence eliminating any chance of their being altered during preparation. The motivation behind the work was to investigate the crystal structure of oxide films with various thicknesses (~ 5 to 2000 nm) and determine the thicknesses at which the oxide films transform from the t-to-m phase. Near the oxide/metal interface, the oxide layer may exist in its untransformed t phase due to high compressive stresses, and therefore, may be more protec-

* Corresponding author. Fax: +1-613 584 3250.

[1] Present address: 1427 E. 30th Ave., Vancouver, BC, V5N 3A1, Canada.

PII S0022-3115(96)00754-4

tive (or less porous) than the transformed outer oxide layer.

2. Experimental

Samples of Zr–2.5 Nb (5 mm diameter × 0.5 mm thickness) were cut from an as-received rod (α-Zr + β-Zr). Similar samples were also cut from a β-annealed (annealed at 1123 K for 1 hour and cooled to ambient temperature within about 30 minutes to obtain the alloy in the β-Zr phase) Zr–20 Nb rod. The alloys were obtained from Teledyne Wah Chang, Albany. All the impurities were quoted to be less than 100 ppm by weight except for Ta, Fe and O which were about 200, 450 and 1000 ppm respectively. The samples were all finely polished using 50 nm alumina. The fine polishing was necessary to obtain good reflection electron diffraction patterns. Even electropolishing the finely polished samples or cleaning them by Ar^+ ion sputtering alters their surface to the extent that hardly any electron diffraction patterns can be obtained. After fine polishing the samples were oxidized in air at a variety of temperatures for different periods to grow oxide films ranging from 5 to 2100 nm in thickness. A number of the samples were also anodically oxidized in 0.18 M KOH under constant current conditions. Details about the samples examined are given in Table 1.

The electron diffraction patterns from the surfaces of the samples were obtained using a Phillips TM300 electron microscope in the reflection mode. The diffraction patterns obtained from a number of gold coated finely polished samples were used to calibrate the microscope. The microscope was used with 60, 80 and 100 keV electrons, but the best diffraction patterns were obtained using the 100 keV electrons (wavelength = 0.0037 nm). With such short wavelengths the Bragg angles are less than 1° and the beam has to strike the surface of the sample at a grazing angle, otherwise the diffracted beam would be blocked by the sample itself. This is why a finely polished surface is needed. The grazing angle geometry also ensures that the penetration depth of the electrons is not more than a few tens of nm, making this technique a highly surface sensitive one. In later sections it will be shown that the penetration depth in our measurements was less than 15 nm.

Fourier transform infrared spectroscopy (FTIR) [8] and scanning Auger microscopy (SAM) were used to measure the thickness of the oxide films and X-ray diffraction (XRD) was used to analyze the crystal structure of the underlying alloys and some of the thick oxide films.

3. Results and discussion

SEM examination of thin oxides showed smooth surfaces. The thick oxides (~ 200 nm) displayed mostly smooth surfaces with some artifacts which at closer examinations proved to be micro pores and fine cracks (Fig. 1 and Fig. 2). Secondary X-ray emission analysis of the regions with pores and cracks showed Al enrichment of about 2–3 at.%.

Although the specimens were oxidized in air, analyses of the them by (SAM) showed no contamination with nitrogen. This was expected due to the fact that the oxidation temperatures were never exceeded 673 K;

Table 1
Principal characteristics of the specimens

Sample	Alloy	Surface condition before oxidation	Oxidation procedure	Oxide thickness (nm)
1676	Zr–2.5 Nb	Polished to 50 nm Al_2O_3	None	9
1677	Zr–2.5 Nb	Polished to 50 nm Al_2O_3 and electopolished	None	8
2143	Zr–2.5 Nb	Polished to 50 nm $Al_2O_3$and gold coated	None	–
2144	Zr–2.5 Nb	Polished to 50 nm Al_2O_3	Anodized, 10 V	25
2147	Zr–2.5 Nb	Polished to 50 nm Al_2O_3	Anodized, 40 V	100
2150	Zr–2.5 Nb	Polished to 50 nm Al_2O_3	523 K air, 24 h	50
2158	Zr–2.5 Nb	Polished to 50 nm Al_2O_3	573 K air, 66 h	200
2164	Zr–2.5 Nb	Polished to 50 nm Al_2O_3	523 K air, 2 h	23
2167	Zr–2.5 Nb	Polished to 50 nm Al_2O_3	Anodized, 40 V	100
2183	Zr–2.5 Nb	Polished to 50 nm Al_2O_3	623 K air, 7 days	800
2189	Zr–2.5 Nb	Polished to 50 nm Al_2O_3	673 K air, 71 h	1800
2728	Zr–20 Nb	Annealed at 1123 K for 1 hour and polished to 50 nm Al_2O_3	473 K air, 0.5 h	20
2731	Zr–20 Nb	Annealed at 1123 K for 1 hour and polished to 50 nm Al_2O_3	623 K air, 18.5 h	2100
2738	Zr–20 Nb	Annealed at 1123 K for 1 hour and polished to 50 nm Al_2O_3	523 K air, 2 h	140
2743	Zr–20 Nb	Annealed at 1123 K for 1 hour and polished to 50 nm Al_2O_3	None	15
2797	Zr–20 Nb	Annealed at 1123 K for 1 hour and polished to 50 nm Al_2O_3 and sputter cleaned by an Ar beam	None	15

ZrN/ZrO_2 system is normally prepared at much higher temperatures [9]. Since the specimens were polished with alumina, a number of them were also examined with SAM for Al contamination. They all showed a thin surface layer (10–40 nm thick) with ~20% Al and the Auger signal indicated that the Al is in the form of Al_2O_3. In general, Zr–20 Nb specimens had more and deeper contamination with alumina than the Zr–2.5 Nb specimens. Nevertheless, due to the following reasons, we believe the alumina contamination has not significantly affected the results:

- solubility of Al_2O_3 in ZrO_2 is extremely small at temperatures below 1800 K [10],
- no Al_2O_3 or Al lines were observed in the RHEED patterns,
- the as-polished Zr–2.5 Nb specimen showed strong α-Zr pattern (see below), and
- although the oxidized Zr–2.5 Nb and Zr–20 Nb specimens both showed surface alumina contamination, they displayed different RHEED patterns.

In Fig. 3 diffraction patterns from a gold coated Zr–2.5 Nb sample and from a Zr–20 Nb sample with ~2100 nm oxide film are displayed. The original negative plates used in the analyses were much sharper than the prints displayed here. To increase resolution and accuracy, the negative plates were scanned by a micro-optical-densitometer and the diffraction patterns presented in the subsequent figures are the results of such scans.

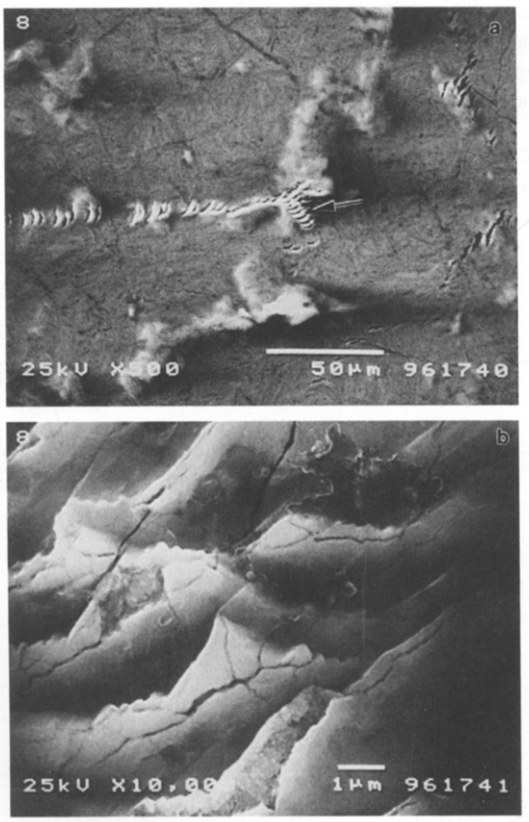

Fig. 1. Scanning electron micrographs of a 1800 nm thick oxide film formed on a Zr–2.5 Nb specimen. The oxide film was grown in air at 673 K. The arrow in (a) is pointing at the spot where micrograph (b) was obtained.

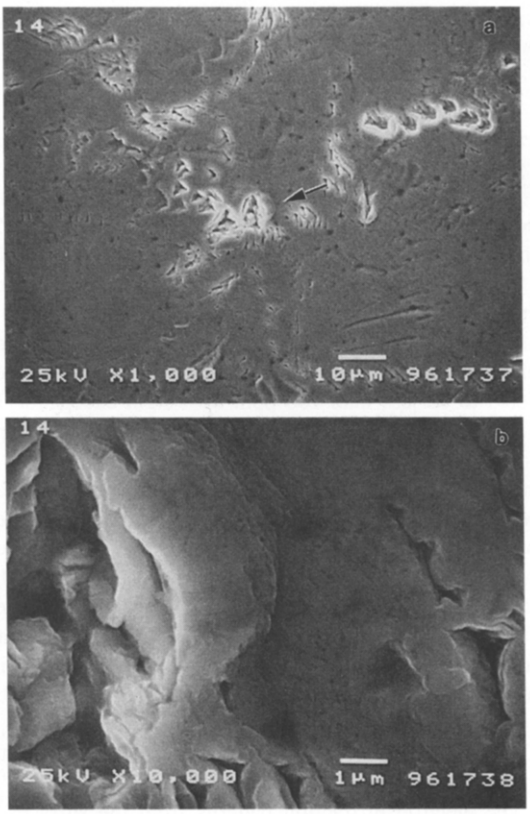

Fig. 2. Scanning electron micrographs of a 2100 nm thick oxide film formed on a Zr–20 Nb specimen. The oxide film was grown in air at 623 K. The arrow in (a) is pointing at the spot where micrograph (b) was obtained.

Every time the microscope was used to obtain the diffraction pattern of a set of specimens, a diffraction pattern of a gold coated sample was also obtained to calibrate the microscope for that specific set. A typical example of a gold diffraction pattern is given in Fig. 4. A minimization routine was written in the C language to analyze the gold pattern and obtain the best value for the microscope 'camera-constant', λL (λ is the electron wavelength and L is the distance from the specimen to the photographic plate). The function to be minimized had two variable parameters; λL and C_0, a value correcting for the offset in the centre of the diffraction pattern. To test the routine, several scans of a photographic plate were made with different points chosen as the centre of the semi-circular patterns. The application of the minimization routine to the patterns obtained from such intentionally off-centred scans resulted in a unique camera-constant proving that a

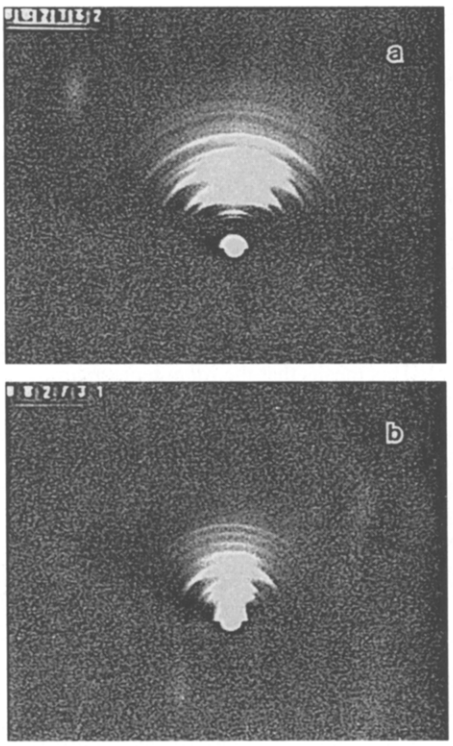

Fig. 3. Reflection electron diffraction patterns obtained from (a) a gold coated Zr–2.5 Nb specimen and (b) a β-annealed Zr–20 Nb specimen with 2100 nm oxide film. The patterns were obtained using a Phillips TM300 electron microscope in the reflection mode.

small error in choosing the centre of the pattern will not seriously affect the final results. The camera-constants resulting from this procedure were used in analyzing the diffraction patterns obtained from the Zr–Nb specimens.

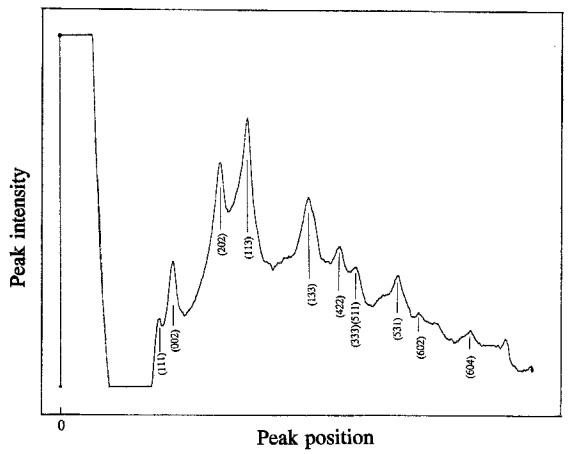

Fig. 4. Micro-optical-densitometer scan of a diffraction pattern obtained from a gold coated metal specimen. The scan was obtained using a Joyce Loebl microdensitometer.

3.1. The Zr–20 Nb specimens

In Fig. 5 the diffraction patterns from three Zr–20 Nb specimens are displayed. The first pattern is from a polished sample with only the oxide formed at room temperature during polishing and storage. This specimen was expected to give a β-Zr diffraction pattern, however as the Fig. 5 shows, the pattern is identical to the other two diffraction patterns obtained from samples with 140 and 2100 nm oxide films. Similar diffraction patterns not shown here were also obtained from oxide films of intermediate thicknesses. These patterns fit to a nearly-cubic-tetragonal (nct) structure with the lattice parameters $a = 5.05$ nm, $c = 5.14$ nm and $c/a = 1.018$ (comparable tetragonalities have also been observed in $ZrO_2/YTaO_4$ and $ZrO_2/(Y_2O_3–Nb_2O_5)$ systems [11,12]). Subsequent analysis of the polished sample by SAM gave an oxide layer of ~ 15 nm (Fig. 6). Since no discernible β-Zr lines are apparent in the pattern, one could conclude that the penetration depth of the 100 keV electrons must be less than 15 nm, which is in accord with earlier results of ~ 6 nm for 60 keV electrons [13].

These results are in good agreement with the results from oxidized β-annealed Zr–20 Nb specimens obtained by TEM, RS and XRD methods [14,15]. In addition, due to highly surface sensitive nature of RHEED, they show that the surface of the oxide even at 2100 nm thickness has not

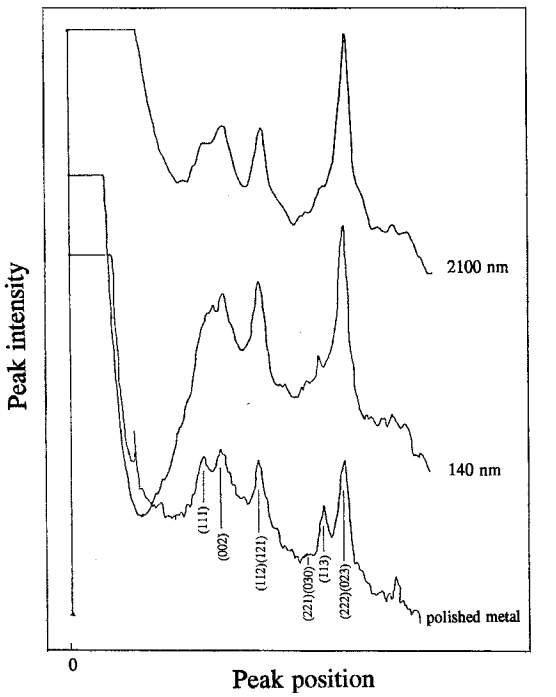

Fig. 5. Micro-optical-densitometer scans of the diffraction patterns obtained from three β-annealed Zr–20 Nb specimens with oxide films of different thicknesses.

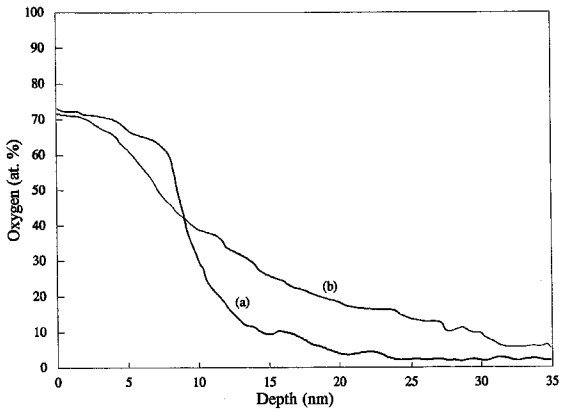

Fig. 6. Oxygen depth profiles of (a) airformed oxide on a polished Zr–2.5 Nb specimen and (b) airformed oxide on a polished Zr–20 Nb specimen. The profiles were obtained by monitoring the oxygen KLL peak using a Physical Electronics Φ-670 scanning Auger microprobe.

transformed to any other structure and that the minor m phase seen by XRD and RS [14,15] is due to the transformation of the underlying alloy during thermal oxidation [16]. In other words, during oxidation the *meta*-stable β-Zr alloy transforms to other components including ω-, $\beta_{\text{Nb-enriched}}$-phase, α-Zr and β-Nb [7] depending on the temperature and duration of the oxidation period. And in turn the oxidation of the α-Zr or possibly other components of the transformed alloy result in the m phase of the inner oxide layer. Thus one may state that the oxide produced as a result of the oxidation of yet untransformed β-Zr phase (Zr–20 Nb) alloy is a stabilized oxide and that its structure stays unchanged at room temperature. This statement also applies to much thicker oxides where the layer close to the surface is formed at early stages from the β-Zr phase. It seems that ~ 20 wt% Nb homogeneously dissolved in zirconium causes the oxide to be stabilized in the nearly-cubic structure, much like the stabilized zirconia structures observed in the zirconia/yttria, zirconia/calcia, $ZrO_2/YTaO_4$ and $ZrO_2/(Y_2O_3–Nb_2O_5)$ systems [11,12,17].

These results are also consistent with interpretation of hydrogen diffusion measurements in thin oxide films grown on β-annealed Zr–20 Nb specimens [18] which showed that such oxide films are a homogeneous and possibly single-phase medium as opposed to the oxides grown on pure Zr [18,19], Zr–1 Nb and Zr–2.5 Nb alloys which are inhomogeneous and multi-phase.

In accord with the present results, it has also been shown [8] that the refractive index of the oxide formed on annealed Zr–20 Nb (β-Zr) is much higher than the refractive index of the oxides formed on α-Zr and that oxides grown on aged Zr–20 Nb (α-Zr + β-Nb) have similar refractive index to that of α-Zr oxide. This indicates that the nct oxide has different electronic structure than the m ZrO_2. These results also emphasize the fact that the nct oxide structure will only form if the niobium in the alloy is completely in solid solution in zirconium and that any precipitation of the β-Nb and the α-Zr will result in mixed oxide structures.

3.2. The Zr–2.5 Nb specimens

Fig. 7 is a diffraction pattern obtained from a polished Zr–2.5 Nb specimen with room temperature oxide. In contrast to the pattern from a polished Zr–20 Nb sample (Fig. 5), the major lines on this pattern fit the α-Zr structure. This means that the room temperature oxide on a Zr–2.5 Nb sample must be much thinner than 15 nm. In fact, analysis by SAM gave a thickness of ~ 9 nm (Fig. 6). The very weak lines fit closely to the nct structure described above (Fig. 5). No m or conventional t lines are discernible. However, they could be masked by the strong α-Zr lines. Similarly, Fisher [20] observed α-Zr lines examining as-polished surface of iodide zirconium by RHEED. In contrast, Alderson [21], also using RHEED, observed only monoclinic ZrO_2 on as-abraded, as-chemically polished or as-electropolished Zr specimens. It is possible that Alderson's specimens had a surface oxide layer, but they give no reason for the discrepancy.

In Fig. 8 the diffraction patterns from five Zr–2.5 Nb specimens with 20, 50, 200, 800 and 1800 nm thick oxide films are displayed. The figure clearly shows that the nct (111) and, with somewhat lower intensity, the nct (222) lines are present in the 20, 50 and 200 nm thick oxide samples. The position of (111) line is closer to the similar

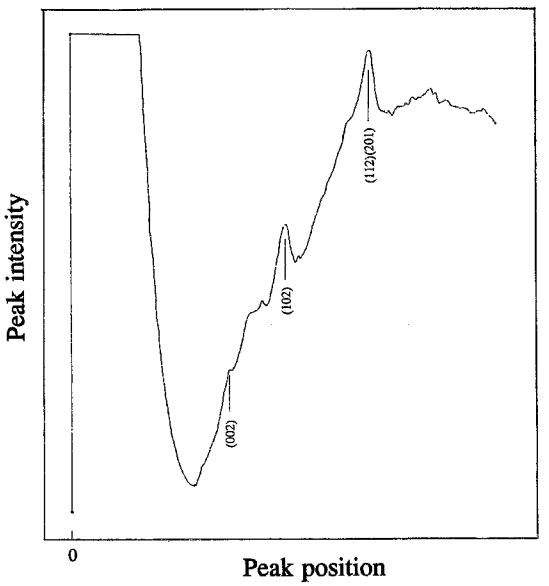

Fig. 7. Micro-optical-densitometer scan of a diffraction pattern obtained from a polished Zr–2.5 Nb specimen with an airformed oxide film.

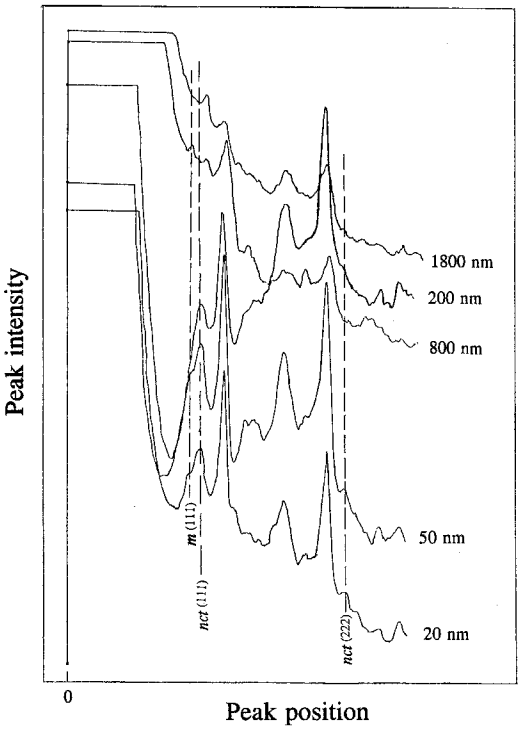

Fig. 8. Micro-optical-densitometer scans of the diffraction patterns obtained from five Zr–2.5 Nb specimens with oxide films of different thicknesses. Notice that the patterns identified by 200 and 800 nm overlap.

line in Fig. 5 ($d = 0.293$ nm) than the conventional t (111) line ($d = 0.296$ nm) [3] and hence they have been assigned to the nct structure. The rest of the peaks on Fig. 8 can be matched with the lines from m, t and nct structures [14,15]. Even the m (111) line is apparent on the pattern from 20 nm oxide sample indicating that the very thin oxide films contain a m component. However, due to texture effects the fraction of the different structures could not be evaluated. In general, these patterns show that oxides grown on Zr–2.5 Nb alloy have a mixture of nct and m crystal structures at thicknesses of 200 nm or less and predominantly a m structure for thicknesses above 800 nm. (Oxide films with 200–800 nm thickness have not been examined). This suggests that the oxide transforms at a film thickness between 200 and 800 nm and that the thickness of the 'protective layer' may have a lower limit of 200 nm. These values agree with the value of ~600 nm obtained by Raman spectroscopy [3] discussed in the introduction. However, the crystal structure of the second phase oxide seems to be closer to nct reported by Woo et al. [15] than t reported by Godlewski et al. [3].

Fisher [20] observed monoclinic and cubic zirconium dioxide patterns examining the surface of zirconium specimens, oxidized in carbon dioxide at 673 and 973 K, using RHEED. Draper and Harvey [13] have also observed cubic Zr_2O examining thin anodic films (< 40 nm thick) grown in dilute sulphuric and nitric acids. Their results also showed that as the oxide film thickness increased a mixture of cubic and monoclinic lines appeared in the RHEED pattern. The cubic structure observed in these early works may be the nct phase observed in the present study, however, a proper comparison can not be made due to the fact that the thickness of the oxide layers and the lattice parameter of the cubic oxide structure or the d-spacings of the diffraction lines were not well specified. In addition, Draper and Harvey [13] showed that anodic films formed in 100% sulphuric acid exhibited only diffuse pattern. In the present investigation the diffraction patterns obtained from the anodically oxidized specimens had generally lower intensity than the ones obtained from thermally grown oxides. They were also more diffuse, indicating that the anodic oxides are under high stress and may be nearly amorphus. The condition was worse for thinner oxide films (25 nm) than the thicker ones.

4. Conclusions

The crystal structure of thin oxide films grown on Zr–2.5 Nb (α-Zr + β-Zr) and Zr–20 Nb (β-Zr) alloys have been studied by the highly surface sensitive reflection high energy electron diffraction technique. The results show that the crystal structure of the oxides grown on Zr–2.5 Nb material change from a mixture of nearly-cubic-tetragonal and monoclinic to only monoclinic at some oxide film thicknesses between 200 and 800 nm. However, the oxide films grown on Zr–20 Nb (β-Zr) have stabilized nearly-cubic-tetragonal structure regardless of the film thickness for oxide films up to 2100 nm investigated here. These results are in good agreement with the previous investigations by X-ray diffraction and Raman Spectroscopy. In addition, they show that the minor monoclinic oxide phase observed in the case of annealed Zr–20 Nb (β-Zr) by other techniques is not present near the surface of the oxide layer. It may result from the transformation of the underlying alloy during the thermal oxidation step rather than the transformation of the oxide itself.

Acknowledgements

We thank V.C. Ling, J.F. Watters and J.E. Winegar for their technical assistance. We also wish to thank L.G.J. Laurin, K.Z. Botros and O.T. Woo for their assistance with the operation of TM300. Critical review of the paper by V.F. Urbanic is appreciated. We also thank the reviewers for their helpful suggestions to improve the manuscript. This work was funded by Candu Owners Group Working Party #35 under WPIR 6609.

References

[1] C. Roy and G. David, J. Nucl. Mater. 37 (1970) 71.
[2] D.H. Bradhurst and P.M. Heuer, J. Nucl. Mater. 37 (1970) 35.
[3] J. Godlewski et al., ASTM-STP-1132 (1991) p. 416.
[4] J. Godlewski, ASTM-STP-1245 (1994) p. 663.
[5] C.E. Ells, Canadian Metallurgical Society Annual Volume 17 (1978) 32.
[6] J.P. Abriata and J.C. Bolcich, Bul. Alloy Phase Diagrams 3 (1982) 1711.
[7] B.A. Cheadle and S.A. Aldridge, J. Nucl. Mater. 47 (1973) 255.
[8] M. Vaillancourt, D. Khatamian and M.A. Maguire, J. Nucl. Mater. 227 (1995) 58.
[9] G. van Tendeloo, L. Anders and G. Thomas, Acta Metall. 31 (1983) 1611.
[10] E.M. Levin and H.F. McMurdie, in: Phase Diagrams for Ceramists — 1975 Supplement, ed. M.K. Reser (American Ceramic Society, Columbus, OH, 1975) p. 135.
[11] T.-S. Sheu, J. Am. Ceram. Soc. 76 (1993) 1772.
[12] D.-J. Kim, J. Am. Ceram. Soc. 73 (1990) 115.
[13] P.H.G. Draper and J. Harvey, Acta Metall. 11 (1963) 873.
[14] Y.P. Lin et al., in: Proc. Mater. Res. Soc. Symp. Ser. 343 (1994) 487. Conference held in San Francisco, CA, USA, Apr. 4–8, 1994.
[15] O.T. Woo et al., in: Proc. Mater. Res. Soc. Symp. Ser. 357 (1995) 219. Conference held in Boston, MA, USA, Nov. 27–Dec. 2, 1994.
[16] V.F. Urbanic et al., ASTM-STP-1245 (1994) p. 116.
[17] K. Nassan, Lapidary J. 31 (1977) 900.
[18] D. Khatamian, Z. Phys. Chem. 181 (1993) 435.
[19] D. Khatamian and F.D. Manchester, J. Nucl. Mater. 166 (1989) 300.
[20] D. Fisher, in: Proc. Eur. Reg. Conf. on Electron Microscopy, Delft, Netherlands, Vol. 1 (1960) p. 293.
[21] R.H. Alderson, in: Proc. Eur. Reg. Conf. on Electron Microscopy, Delft, Netherlands, Vol. 1 (1960) p. 297.